Check for updates

CO_2 Reduction Reaction

How to cite:
International Edition: doi.org/10.1002/anie.202300129
German Edition: doi.org/10.1002/ange.202300129

Suppressive Strong Metal-Support Interactions on Ruthenium/TiO_2 Promote Light-Driven Photothermal CO_2 Reduction with Methane

*Qiang Li, Huiling Wang, Meng Zhang, Guanghui Li, Jing Chen, and Hongpeng Jia**

Abstract: Strong metal-support interactions (SMSI) have gained great attention in the heterogeneous catalysis field, but its negative role in regulating light-induced electron transfer is rarely explored. Herein, we describe how SMSI significantly restrains the activity of Ru/TiO_2 in light-driven CO_2 reduction by CH_4 due to the photo-induced transfer of electrons from TiO_2 to Ru. In contrast, on suppression of SMSI Ru/TiO_2–H_2 achieves a 46-fold CO_2 conversion rate compared to Ru/TiO_2. For Ru/TiO_2–H_2, a considerable number of photo-excited hot electrons from Ru nanoparticles (NPs) migrate to oxygen vacancies (OVs) and facilitate CO_2 activation under illumination, simultaneously rendering $Ru^{\delta+}$ electron deficient and better able to accelerate CH_4 decomposition. Consequently, photothermal catalysis over Ru/TiO_2–H_2 lowers the activation energy and overcomes the limitations of a purely thermal system. This work offers a novel strategy for designing efficient photothermal catalysts by regulating two-phase interactions.

Introduction

Strong metal–support interactions (SMSI) are a common effect in supported metal catalysts, which refers to support-derived species migrating onto the surface of metal nanoparticles (NPs) to form an ultrathin encapsulation layer.[1] This process has been extensively studied in thermal catalytic and electric catalytic systems to elucidate the structure–activity relationship, but the mechanism of influence remains elusive in photocatalytic and photothermal catalytic systems.[2] Recent works demonstrate that SMSI can affect light-driven photocatalytic properties due to the formation of encapsulation layers.[3] As previously reported, SMSI occurrence in Pd/TiO_2 catalysts facilitates photo-induced electron transfer from TiO_2 to the adjacent Pd species and thus benefits the activation of acetylene.[4] The unique coordination structure and electronic properties of Pt-I_3 species contribute to the SMSI effect, boosting photo-generated electron transfer from Cs_2SnI_6 to Pt single atoms and eventually accelerating the kinetics for hydrogen production.[5] In these cases, SMSI promotes the enrichment of photo-generated electrons from semiconductors to metal NPs, leaving metal NPs mainly in an electron-sufficient state and improving the catalytic activity. On the other hand, since the Fermi level of the partially reduced oxides is higher than that of metal NPs, the classical SMSI results in electron transfer from supports to metals to achieve Fermi-level equilibration, ultimately establishing electron-rich active sites.[6] Nevertheless, for a reaction dependent on electron-deficient active sites, a profound exploration is required to ascertain whether the migration of electrons to metal NPs boosted by SMSI is favorable to catalytic processes.

Solar-driven dry reforming of methane (DRM: $CO_2+CH_4\rightarrow 2H_2+2CO$) is an environmentally friendly and effective method to synchronously resolve climate emergencies and energy crises.[7] Some important progress has presented that electron-deficient sites on metal surfaces serve as active sites for dissociating the C–H bond of CH_4, which is the rate-determining step of DRM reaction processes.[8] However, few studies have been conducted to tailor the light-driven DRM catalytic activity by tuning the chemical state of the metal NPs. Recent work shows hot electrons excited from interband transition on Rh NPs can rapidly migrate to TiO_2 and leave Rh species in an electron-deficient state, promoting the breakage of the C–H bond during photo-induced steam reforming of methane.[9] This inspired us to adjust the transfer process of photo-induced carriers under light irradiation to finely modulate the surface electronic state of metal nanostructures and finally boost the light-driven DRM reaction activity. Considering that the classical SMSI effect occurring in supported metal catalysts increases the electron density of metal NPs under illumination, inhibiting the SMSI effect may be conducive to

[*] Q. Li, H. Wang, M. Zhang, G. Li, H. Jia
Xiamen Key Laboratory of Materials for Gaseous Pollutant Control, Institute of Urban Environment, Chinese Academy of Sciences
361021 Xiamen (China)
and
CAS Center for Excellence in Regional Atmospheric Environment, and Key Laboratory of Urban Pollutant Conversion, Institute of Urban Environment, Chinese Academy of Sciences
361021 Xiamen (China)
E-mail: hpjia@iue.ac.cn
J. Chen
Fujian Institute of Research on The Structure of Matter, Chinese Academy of Sciences
350002 Fuzhou (China)
and
Xiamen Institute of Rare-earth Materials, Haixi Institutes, Chinese Academy of Sciences
361021 Xiamen (China)
Q. Li, H. Wang, M. Zhang, G. Li, J. Chen, H. Jia
University of Chinese Academy of Sciences
100049 Beijing (China)

© 2023 Wiley-VCH GmbH

achieving the electron-deficient active sites and facilitating the photothermal DRM reaction.

Inspired by this scenario, we utilized Ru/TiO_2 composites as model catalysts to demonstrate the negative role of the SMSI effect in modulating the electronic structure and catalytic activity in the light-driven photothermal DRM reaction. Impressively, Ru/TiO_2 shows poor activity due to the SMSI effect, while Ru/TiO_2–H_2 profits from the suppressive SMSI and exhibits an enhanced CO_2 conversion rate 46-fold that of Ru/TiO_2. The characterization of charge-transfer processes confirms that the suppressed SMSI effect promotes the light-induced hot electrons on Ru NPs to be injected into the TiO_2–H_2 support over Ru/TiO_2–H_2, contributing to the electron-deficient state of Ru NPs and promoting the activation of CH_4. Moreover, the light-induced electrons can be captured by the surface oxygen vacancies (OVs) of TiO_2–H_2 and further react with CO_2 molecules. As expected, Ru/TiO_2–H_2 presents the lower activation energy in the photothermal DRM reaction and overcomes the limitations of a purely thermal system. This work provides vivid evidence for the delicate modulation of the catalyst's electronic structure to achieve an efficient light-driven photothermal reaction.

Results and Discussion

Ru/TiO_2–H_2 was prepared directly by impregnating $RuCl_3$ solution into a H_2-pretreated commercial TiO_2 (P25) support following calcination in H_2 (Figure 1a), and Ru/TiO_2 was synthesized by the same procedure except for employing commercial TiO_2 as the support. The X-ray fluorescence

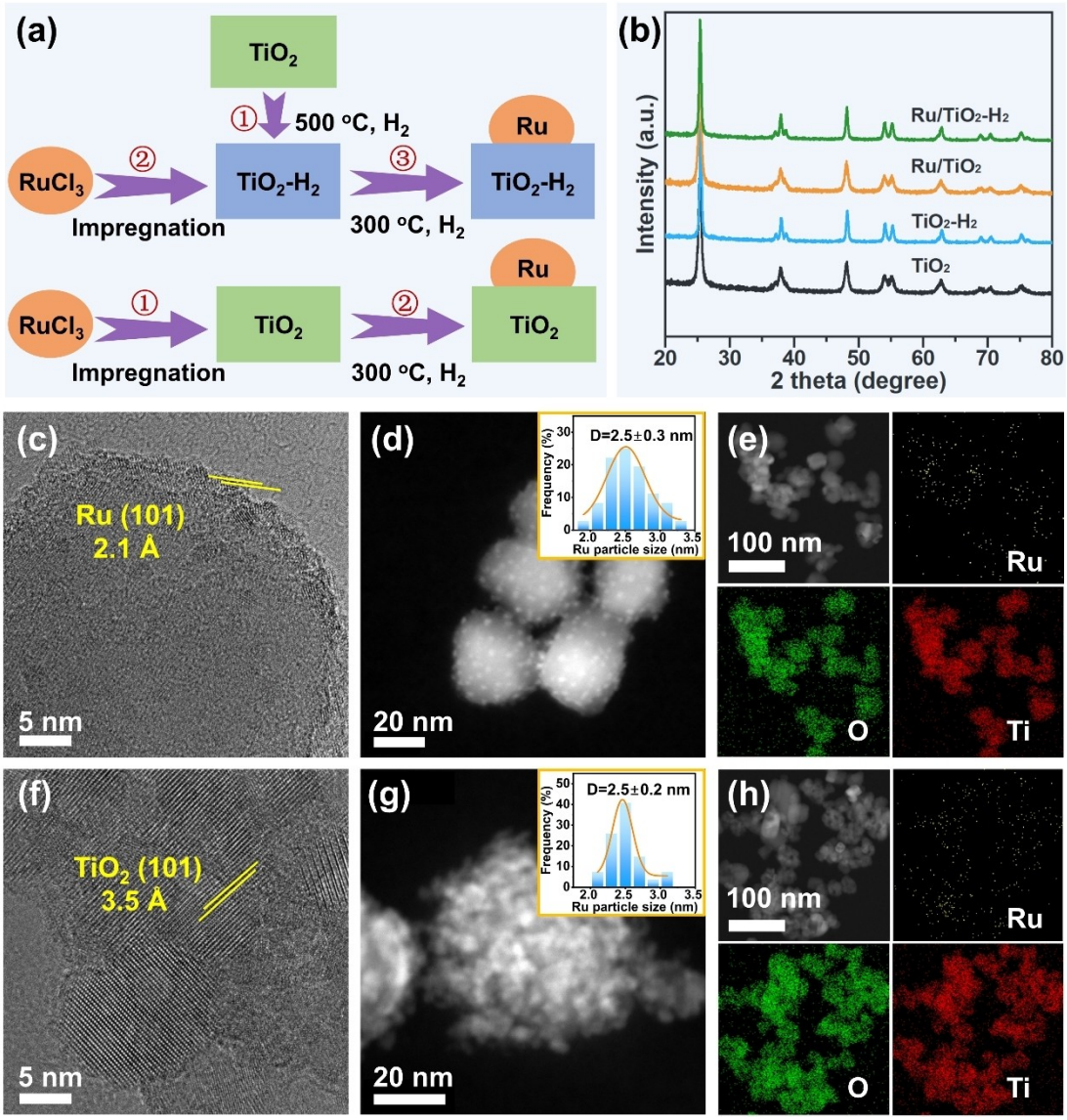

Figure 1. a) Illustration of the synthesis process of Ru/TiO_2–H_2 and Ru/TiO_2. b) XRD patterns of TiO_2–H_2, TiO_2, Ru/TiO_2–H_2, and Ru/TiO_2. c)–e) HRTEM, STEM, and EDS element mapping images of Ru/TiO_2–H_2, respectively. f)–h) HRTEM, STEM, and EDS element mapping images of Ru/TiO_2, respectively. The inset plots int the STEM images (d) and (g) are the particle size distribution of Ru NPs.

© 2023 Wiley-VCH GmbH

15213773, 0, Downloaded from https://onlinelibrary.wiley.com/doi/10.1002/anie.202300129 by Cas-Institute Of Urban Environment, Wiley Online Library on [31/03/2023]. See the Terms and Conditions (https://onlinelibrary.wiley.com/terms-and-conditions) on Wiley Online Library for rules of use; OA articles are governed by the applicable Creative Commons License

(XRF, Table S1) technique was firstly performed to confirm the existence of the Ru element and determine the Ru loading to be 0.9 wt % for Ru/TiO_2–H_2 and 1.2 wt % for Ru/TiO_2, respectively. The X-ray diffraction (XRD) patterns (Figure 1b) of both Ru-containing catalysts show no detectable peaks for Ru species, which demonstrates that Ru species are highly dispersed and of small size.[10] In addition, Ru/TiO_2–H_2 displays the sharp and narrow peak associated with the TiO_2 phase, indicating that pre-reduction in hydrogen leads to larger TiO_2 crystalline sizes. Consequently, Ru/TiO_2–H_2 displays a decreased specific surface area (S_{BET} = 62.2 $m^2 g^{-1}$) in comparison to Ru/TiO_2 (S_{BET} = 107.6 $m^2 g^{-1}$), as depicted in Figure S1. High-resolution transmission electron microscopy (HRTEM) of Ru/TiO_2–H_2 (Figure 1c) presents a fringe spacing of 2.1 Å, corresponding to the d-spacing of Ru (101). Moreover, Ru exists as NPs over Ru/TiO_2–H_2 with an average size of 2.5 nm, as shown in the scanning transmission electron microscopy (STEM) image and particle size distribution pattern (Figure 1d). The energy-dispersive X-ray spectroscopy (EDS) mapping images (Figure 1e) show a homogeneous distribution of Ru, Ti, and O elements on Ru/TiO_2–H_2. For Ru/TiO_2, only the lattice spacing for TiO_2 (101) planes can be observed in HRTEM patterns (Figure 1f). The STEM image (Figure 1g) shows that a visible covering exists on the Ru NPs with a similar size distribution of Ru NPs compared to that of Ru/TiO_2–H_2, and EDS mapping images (Figure 1h) reveal the homogeneous distribution. The covering on Ru NPs is attributed to an SMSI effect whereby TiO_x migrates to Ru NPs, initiating at a reduction temperature higher than 300 °C.[11]

H_2-temperature programmed reduction (H_2-TPR) was employed to give an insight into the metal–support interactions in the Ru catalysts, as presented in Figure 2a. Ru/TiO_2 shows H_2 consumption peaks at 95 °C and 350 °C, which belong to surface RuO_2 and Ru species that strongly interact with TiO_2, respectively. Meanwhile, the dominant peaks at 420 °C and 530 °C are ascribed to H_2 consumption by surface TiO_2. Ru/TiO_2–H_2 displays much stronger signals at 84 °C and 157 °C, and a weaker signal at 334 °C, indicating the existence of more surface RuO_2 species and weaker interaction between Ru species with TiO_2.[12] The surface Ru sites were characterized via diffuse-reflectance infrared Fourier transform spectroscopy (DRIFTS) utilizing CO as the probe at 25 °C (Figure 2b). Ru/TiO_2 shows four kinds of CO adsorption species on Ru sites. The bands at 2138 and 2070 cm^{-1} are attributed to the multi-carbonyl species adsorbed on Ru sites with low coordination numbers ($Ru(CO)_x$, x = 2, 3).[13] The peaks at 2003 and 1974 cm^{-1} belong to the CO adsorbed on top (Ru–CO) and at the interface between Ru and TiO_2 (Ru_{if}–CO), respectively.[14] Though Ru/TiO_2–H_2 displays identical CO adsorption modes with Ru/TiO_2, the relative intensity of the $Ru(CO)_3$ mode on low-coordinated Ru sites decreases and the signal of Ru–CO enhances, indicating the existence of more interfacial RuO_x species for Ru/TiO_2–H_2. Furthermore, an SMSI effect contributes to more electrons transferred from the TiO_2 support to Ru in the Ru/TiO_2 catalyst, and the transferred electrons into occupied d orbitals of Ru can be back-donated to the π* orbital of CO adsorbed on Ru sites, thus strengthening the Ru–C bond and weakening the strength of the C–O bond.[15] On the contrary, Ru/TiO_2–H_2 with the suppressive SMSI effect shows an enhanced C–O bond and the bands for carbonyl groups of $Ru(CO)_2$, Ru–CO, and Ru_{if}–CO shift to higher wavenumbers. Therefore, the above experiments clarify that the SMSI effect has been weakened and the surface state of Ru species is modified on Ru/TiO_2–H_2. The modified SMSI effect can effectively influence the adsorption–desorption ability to the reactants (CO_2, CH_4) and products (CO, H_2) during the DRM reaction. Both CO_2-temperature-programmed desorption (CO_2-TPD) profiles (Figure S2) of Ru/TiO_2 and Ru/TiO_2–H_2 samples display desorption peaks in three regions: 50–200 °C, 200–400 °C, and 400–600 °C, corresponding to weak, medium, and strong basic sites, respectively. Apparently, Ru/TiO_2 exhibits stronger CO_2 adsorption abilities than Ru/TiO_2–H_2. Analogously, Ru/TiO_2 displays the slightly intensified desorption peak of CH_4 compared to Ru/TiO_2–H_2 (Figure S3). The results manifest that Ru/TiO_2 achieves better adsorption characteristics to the reactants. Nevertheless, the TPD profiles (Figure 2c, d) of the products (CO and H_2) for Ru/TiO_2 also show a significantly enhanced signal compared to that of Ru/TiO_2–H_2, indicating that Ru/TiO_2 possesses much weaker desorption capacity to the products, which is not favorable to a further DRM reaction. Therefore, the SMSI effect in Ru/TiO_2 contributes to better adsorption ability to the reactant, but meanwhile, is not conducive to desorption of the products, thus inhibiting the continuation of the catalytic process and reducing the reaction activity and selectivity. In contrast, Ru/TiO_2–H_2 exhibits almost comparable adsorption capacity for reactants and much inferior adsorption ability for products, which can accelerate the departure of product molecules and further offer more unoccupied active sites to continue the reaction. The changed electronic structure of the Ru-loaded composites can significantly impact the optical properties, as shown by the UV/Vis diffuse reflectance spectroscopy (DRS, Figure 2e). Ru-loaded samples display greatly enhanced absorption of visible and near-infrared light on account of the localized surface plasmon resonance (LSPR) effect of Ru particles. Furthermore, SMSI-induced TiO_x layers on the Ru/TiO_2 catalyst can improve light absorption, and thus Ru/TiO_2 exhibits stronger optical absorption than Ru/TiO_2–H_2. The band gaps obtained by the Kubelka–Munk function of TiO_2, TiO_2–H_2, Ru/TiO_2, and Ru/TiO_2–H_2 are determined to be 3.17, 3.17, 2.73, and 2.96 eV, respectively (Figure S4). Moreover, photoluminescence spectroscopy (PL) spectra (Figure 2f) reveal that the fluorescence intensity of Ru/TiO_2 is lower than that of Ru/TiO_2–H_2, confirming that Ru/TiO_2 can inhibit electron–hole recombination well.[16] These results mean that there is more effective charge separation for Ru/TiO_2 and faster transfer of photo-generated electrons excited from the valence band (VB) to the conduction band (CB) of TiO_2, which can be attributed to the SMSI effect and its role in intensifying the transfer of excited electrons in the CB of TiO_2 to Ru NPs.

To directly evaluate surface charge regulation, Kelvin probe force microscopy (KPFM) analysis was performed to

© 2023 Wiley-VCH GmbH

15213773, 0, Downloaded from https://onlinelibrary.wiley.com/doi/10.1002/anie.202300129 by Cas-Institute Of Urban Environment, Wiley Online Library on [31/03/2023]. See the Terms and Conditions (https://onlinelibrary.wiley.com/terms-and-conditions) on Wiley Online Library for rules of use; OA articles are governed by the applicable Creative Commons License

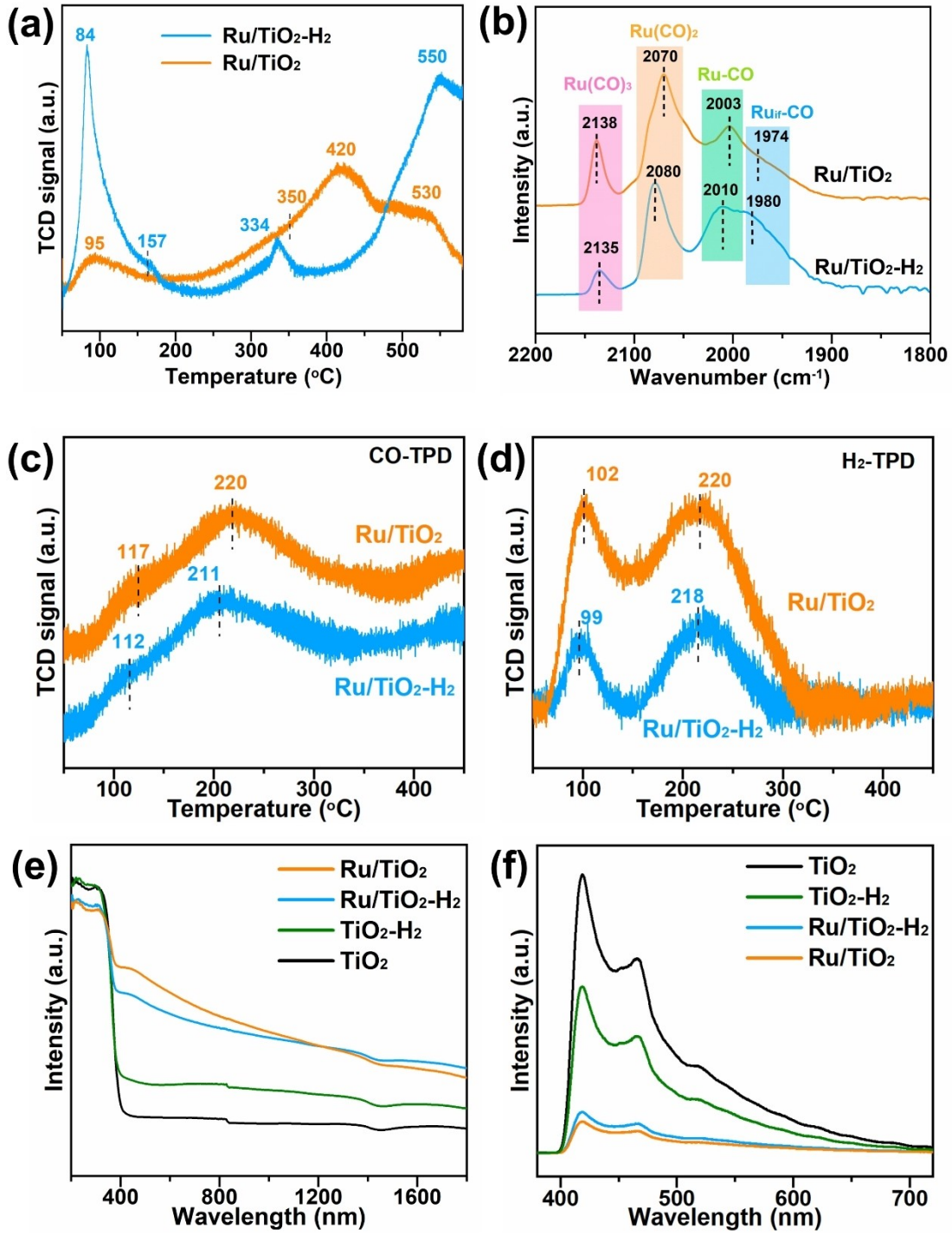

Figure 2. a) H_2-TPR profiles, b) CO-DRIFTS spectra at 25 °C, c) CO-TPD profiles, d) H_2-TPD profiles, e) DRS spectra, and f) steady-state PL spectra (λ_{ex} = 300 nm) of the catalysts.

analyze the surface potential under UV/Vis light irradiation and dark conditions, respectively (Figure 3a, b). The surface potentials are related to the contact potential difference (CPD), and meanwhile, the light-induced difference of ΔCPD signals (Figure 3c, d) is directly correlated to the surface photo voltages (SPV). The larger negative SPV observed on Ru/TiO_2–H_2 (−110 ± 10 mV) compared to that of Ru/TiO_2 (−60 ± 15 mV) infers the enhanced accumulation of electrons on the TiO_2–H_2. This suggests that more electrons are injected from the resonant Ru NPs to TiO_2–H_2 on the Ru/TiO_2–H_2 catalyst, resulting in more negative charge accumulation in the TiO_2–H_2 support and more positive charge accumulation in the Ru NPs. In situ irradiated X-ray photoelectron spectroscopy (ISI-XPS) char-

© 2023 Wiley-VCH GmbH

15213773, 0, Downloaded from https://onlinelibrary.wiley.com/doi/10.1002/anie.202300129 by Cas-Institute Of Urban Environment, Wiley Online Library on [31/03/2023]. See the Terms and Conditions (https://onlinelibrary.wiley.com/terms-and-conditions) on Wiley Online Library for rules of use; OA articles are governed by the applicable Creative Commons License

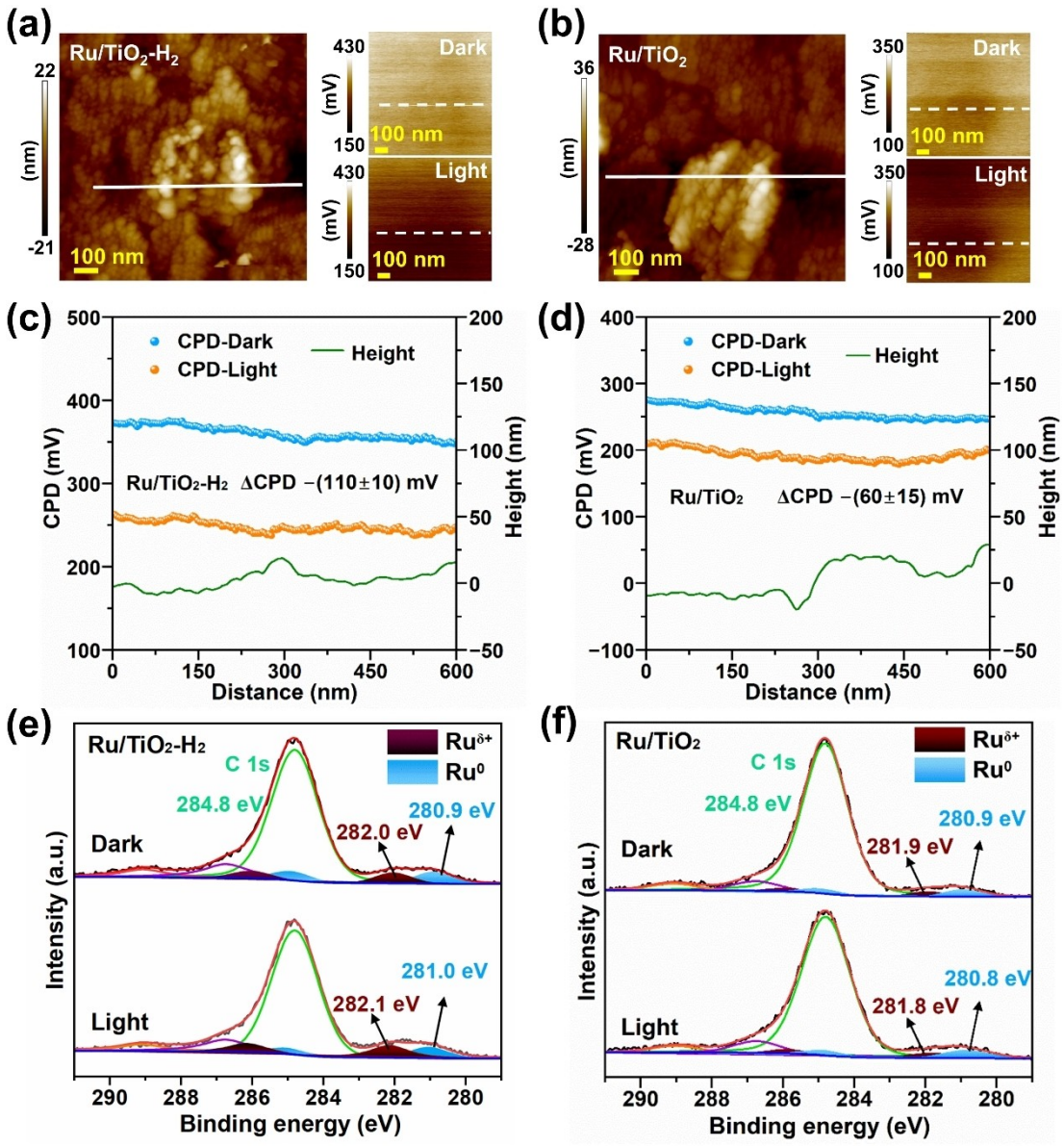

Figure 3. a), b) Surface morphologies and corresponding surface potential images in the absence and presence of light (10–780 nm) for Ru/TiO_2–H_2 and Ru/TiO_2, respectively. c), d) The effect of irradiation on CPD changes along with the height profile of Ru/TiO_2–H_2 and Ru/TiO_2, respectively. e), f) In situ irradiated XPS spectra of Ru 3d for Ru/TiO_2–H_2 and Ru/TiO_2, respectively.

acterization was performed to further demonstrate the light-induced charge transfer process. As depicted in Figure S5a–b, Ti $2p_{1/2}$ of Ru/TiO_2 exhibits a higher binding energy (464.6 eV) than that of Ru/TiO_2–H_2 (464.5 eV), while no obvious shift in Ti 2p binding energy is found upon illumination for two samples. Both Ru $3d_{3/2}$ spectra (Figure 3e, f) of Ru/TiO_2–H_2 and Ru/TiO_2 show oxidized ($Ru^{\delta+}$) and metallic (Ru^0) states. For Ru/TiO_2–H_2, owing to the transfer of more hot electrons from light-induced interband transitions on Ru NPs to TiO_2–H_2, Ru shows a decreased electron density. As a result, the calculated $Ru^{\delta+}/Ru^0$ ratio (Table S2) of Ru/TiO_2–H_2 increases to 1.25 from 0.94, and a positive shift is observed in the Ru 3d binding energy after illumination for 60 min. Nevertheless, as for the Ru/TiO_2 catalyst, the dominant process is that Ru on TiO_2 easily traps photo-excited electrons from the conduction band of TiO_2 due to the SMSI effect, resulting in a higher electron density of Ru atoms and a decreased $Ru^{\delta+}/Ru^0$ ratio (from 0.70 to 0.62) and negative peak shifts under light irradiation. Based on the above analysis, we speculate that different charge-transfer processes occur on Ru/TiO_2–H_2 versus Ru/TiO_2 due to the difference in strength of the metal–support interactions. The SMSI effect endows Ru/TiO_2 with enhanced light-absorption ability and a narrower energy band structure, which then enables transfer of photo-excited electrons from TiO_2 to Ru NPs. Consequently, Ru NPs on Ru/TiO_2 may maintain a higher charge-density state under light irradiation, which is not conducive to methane

© 2023 Wiley-VCH GmbH

15213773, 0, Downloaded from https://onlinelibrary.wiley.com/doi/10.1002/anie.202300129 by Cas-Institute Of Urban Environment, Wiley Online Library on [31/03/2023]. See the Terms and Conditions (https://onlinelibrary.wiley.com/terms-and-conditions) on Wiley Online Library for rules of use; OA articles are governed by the applicable Creative Commons License

activation and cleavage. In contrast, the present Ru/TiO_2–H_2 system under light irradiation mainly exhibited plasmon-induced charge separation, thus leaving the Ru surface with an electron-deficient state to promote C–H bond activation and enhance the catalytic properties for photothermal DRM.[9]

Light-driven photothermal DRM was performed in a flow reactor without external heating using focused full spectrum irradiation (light intensity = 12.0 W cm^{-2}, Figure S6). No CO and H_2 products were detected during the DRM reaction on pure TiO_2 and TiO_2–H_2. Ru/TiO_2 shows production rates for CO (r_{CO}) and H_2 (r_{H_2}) of 12.8 mmol g_{cat}^{-1} h^{-1} and 1.4 mmol g_{cat}^{-1} h^{-1}, respectively, and conversion rates of CO_2 (r_{CO_2}) and CH_4 (r_{CH_4}) are 8.7 mmol g_{cat}^{-1} h^{-1} and 7.9 mmol g_{cat}^{-1} h^{-1}, respectively (Figure 4a, b). These results suggest that Ru NPs are essential for triggering the DRM reaction. Interestingly, Ru/TiO_2–H_2 exhibits dramatically enhanced DRM activity by pre-annealing of the TiO_2 support in hydrogen. The r_{CO_2} of Ru/TiO_2–H_2 is 399.7 mmol g_{cat}^{-1} h^{-1}, which is approximately 46-fold higher compared to that of Ru/TiO_2. And r_{CO}, r_{H_2}, and r_{CH_4} of Ru/TiO_2–H_2 also exhibit the higher value of 708.4 mmol g_{cat}^{-1} h^{-1}, 645.5 mmol g_{cat}^{-1} h^{-1}, and 313.4 mmol g_{cat}^{-1} h^{-1}, respectively. This is attributed to the suppressed strong interaction over Ru/TiO_2–H_2 bringing a particular light-induced electronic transfer from Ru to TiO_2–H_2. The isotope-labeling experiment was performed over Ru/TiO_2–H_2 by utilizing $^{13}CO_2$ as a reactant. After the reaction, signals for ^{13}CO ($m/z = 29$) and $^{13}CO_2$ ($m/z = 45$) were detected by mass spectrometry (MS). In addition, the gas chromatogram after DRM reaction (Figure S7) shows a strong peak with a retention time of 1.8 min originating from the CO, indicating that the produced CO is converted from the reactants. In comparison to the reported catalysts in light-involved DRM reactions (Table S1), Ru/TiO_2–H_2 in this work shows good activity at relatively low temperature, simultaneously making full use of solar energy without external heating to drive the catalytic process. Moreover, the reaction rates of Ru/TiO_2–H_2 maintain stable reactivity over 800 min (Figure S8) with the turnover number (TON) estimated to be 34475. According to the HRTEM and element mapping images (Figure S9a–b) of Ru/TiO_2–H_2 after reaction for 800 min, no carbon fiber is detected and the particle size of Ru remains at ca. 2.5 nm with high dispersion. These results suggest that Ru/TiO_2–H_2 can suppress the aggregation of the catalyst and carbon coking during photothermal catalytic DRM reaction. Moreover, the ratio of r_{H_2} and r_{CO}, denoting the selectivity of Ru/TiO_2–H_2, is calculated to be 0.9, which is far superior to the selectivity of Ru/TiO_2 (0.1). It indicates that the reverse water–gas shift

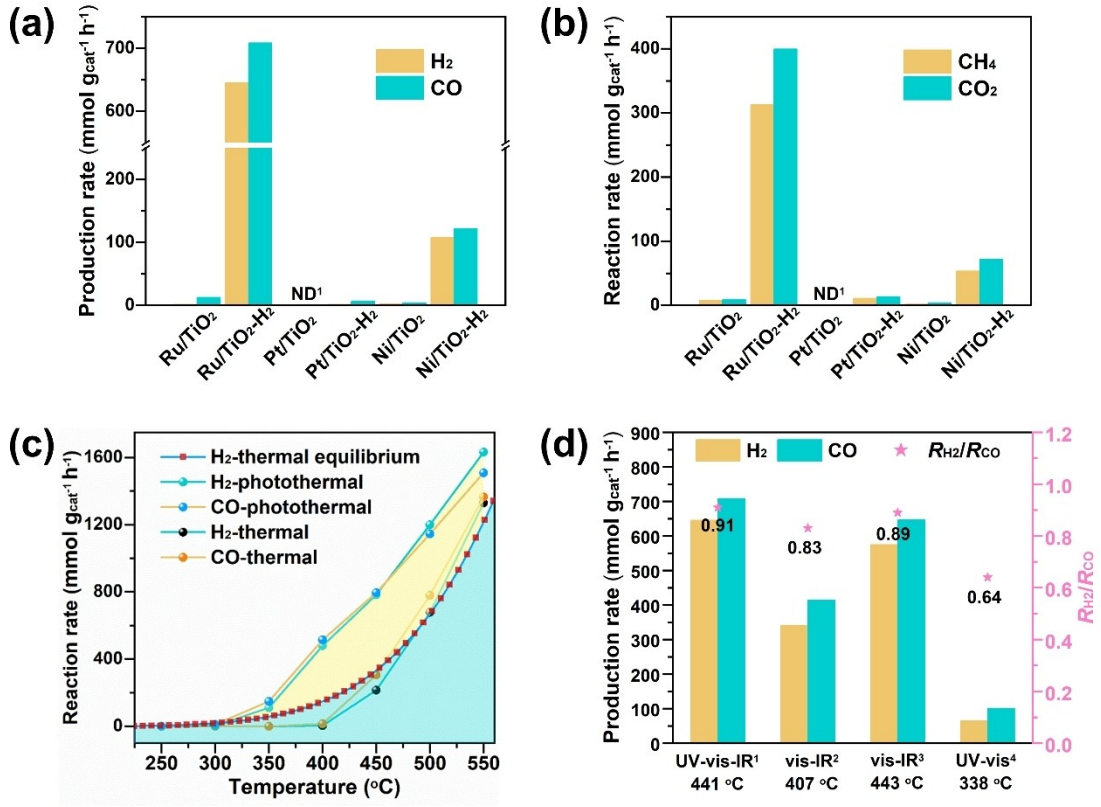

Figure 4. a) Average production rates of H_2 and CO, and b) average reaction rates of CO_2 and CH_4, both under focused full-spectrum light irradiation (12.0 W cm^{-2}) and with a reaction duration of 2 h. c) Rates of H_2 and CO under irradiation or external heating supply as a function of the apparent temperature over Ru/TiO_2–H_2 in flow conditions. d) Production rates of H_2 and CO over Ru/TiO_2–H_2 under illumination of various wavelengths. Reaction conditions: catalyst (5.0 mg), continuous flow (8 vol% CO_2, 8 vol% CH_4, and 84 vol% Ar), rate of 50 mL min^{-1}. ND[1] means "not detected".

© 2023 Wiley-VCH GmbH

15213773, 0, Downloaded from https://onlinelibrary.wiley.com/doi/10.1002/anie.202300129 by Cas-Institute Of Urban Environment, Wiley Online Library on [31/03/2023]. See the Terms and Conditions (https://onlinelibrary.wiley.com/terms-and-conditions) on Wiley Online Library for rules of use; OA articles are governed by the applicable Creative Commons License

reaction ($H_2+CO_2\rightarrow CO+H_2O$) and other secondary reactions are more likely to occur on Ru/TiO_2 during DRM. The results are consistent with the H_2-TPD results (Figure 3d), whereby Ru/TiO_2 displays a stronger adsorption ability of H_2, which may facilitate the side reaction and reduce the selectivity (the ratio of r_{H_2}/r_{CO}) of the DRM reaction. Therefore, Ru/TiO_2–H_2 attained via pre-annealing of TiO_2 in hydrogen can significantly modify not merely the photothermal DRM catalytic activity but also the selectivity. Moreover, such a beneficial effect of the hydrogenated TiO_2 is a general trend in other metals, including noble metal Pt and non-noble metal Ni. As depicted in Figure 4a, b, Pt/TiO_2–H_2 and Ni/TiO_2–H_2 display much higher values of r_{H_2} and r_{CO} compared to that of Pt/TiO_2 and Ni/TiO_2, respectively.

To explore the contribution of the photochemical and light-induced thermal effect to the light-driven DRM process, the performance of Ru/TiO_2–H_2 under different light irradiation intensities and external heating conditions have been investigated. The light intensity and light-induced surface temperature of the catalyst are recorded in Figure S10. The red dotted line (Figure 4c) represents the thermodynamic equilibrium under the same conditions calculated by HSC Chemistry Software, which is the limit of syngas production rates by a thermal catalyst. The thermal DRM catalytic performances of Ru/TiO_2–H_2 in this work are mostly below the thermodynamic equilibrium, whereas the light-driven DRM catalysis over Ru/TiO_2–H_2 exhibits much more superior syngas formation rates than that under thermal conditions, which are even beyond the thermodynamic equilibrium. The results indicate that both photoelectric and photothermal processes are involved in the light-driven DRM reaction on Ru/TiO_2–H_2. Furthermore, the Arrhenius curves of $\ln(r_{CO})$ and $\ln(r_{H_2})$ vs 1/T are plotted according to the production rates of Ru/TiO_2–H_2 under thermal catalysis and photothermal catalysis (Figure S11), respectively, both of which showed a good linear relationship with 1/T. The apparent activation energy (E_a) of CO and H_2 in the light-driven DRM are calculated to be 33.14 kJ mol^{-1} and 37.82 kJ mol^{-1}, respectively, which are significantly lower than those of 74.02 kJ mol^{-1} and 90.22 kJ mol^{-1} under the thermally driven process. As displayed in Figure S12, the H_2/CO ratio in the light-driven DRM catalysis is noticeably higher compared to that in the thermally driven catalysis. The value of the H_2/CO ratio under light irradiation reached 0.9 (near the theoretical value of 1) even at 400 °C, whereas the value was only 0.3 by thermal catalysis. This may be due to the electronic interband transition of Ru, offering sufficient hot electrons to facilitate the generation and desorption of H_2.[17] Hence, it can be concluded that light irradiation in this system does not merely lower the activation energy of the DRM reaction but also inhibits the side reaction during the DRM reaction, and thus enhances the catalytic activity and selectivity.

To distinguish the influence of various wavelength regions on the light-driven DRM reaction, a series of experiments were carried out on the Ru/TiO_2–H_2 catalyst utilizing different filters under 300 W Xe lamp irradiation. As displayed in Figure 4d, after cutting off the IR light, the light intensity and T_{eq} fell to 7.4 W cm^{-2} and 338 °C, respectively. As a result, r_{H_2} drops sharply to 64.8 mmol g_{cat}^{-1} h^{-1}, accounting for one-tenth of the rate under the full-spectrum irradiation. This clarifies that the surface temperature of Ru/TiO_2–H_2 plays a crucial role in the catalytic activity and selectivity, and the IR wavelength is the main contributor of heat for the photothermally catalyzed DRM reaction. When cutting off the UV light, the irradiation intensity decreases to 10.9 W cm^{-2} and T_{eq} is 407 °C. Consequently, the r_{H_2} of Ru/TiO_2–H_2 under vis-IR light (>420 nm) irradiation remains at 341.8 mmol g_{cat}^{-1} h^{-1}. Subsequently, we increased the irradiation intensity to 13.2 W cm^{-2} to achieve a T_{eq} (443 °C) approximate to that under UV/Vis-IR light irradiation (441 °C). Although r_{H_2} achieves a value of 574.5 mmol g_{cat}^{-1} h^{-1} and the H_2/CO ratio reaches 0.89, the performance is lower than that under UV/Vis-IR conditions ($r_{H_2}=645.5$ mmol g_{cat}^{-1} h^{-1}). It suggests that UV light contributes to increasing the catalytic activity and selectivity. Meanwhile, the catalytic activity under vis-IR conditions is much higher than that in external heating conditions with a similar T_{eq} of 450 °C ($r_{H_2}=$ 216.4 mmol g_{cat}^{-1} h^{-1}), demonstrating that the light in the vis-IR region also facilitates the catalytic performance during the light-driven DRM reaction. To discuss which wavelengths contributed to the DRM reaction in more detail, the action spectrum of Ru/TiO_2–H_2 was investigated with different single wavelength irradiations utilizing a bandpass filter at a similar surface temperature (Figure S13). Ru/TiO_2–H_2 presents a much enhanced activity under an incident light of 365, 450, and 500 nm in comparison to dark condition, whereas the yield of H_2 is much lower in 600 nm. The highest H_2 generation rate of 19.0 mmol g_{cat}^{-1} h^{-1} is achieved under an incident light of 365 nm (with a quantum efficiency of 2.3 %). The results show that the band gap excitation of the TiO_2–H_2 support and hot electrons excited by visible light play a crucial role in the enhancement of DRM activity.

Generally, CO_2 is thought to be adsorbed and activated by oxygen vacancies and CH_4 is dissociated by metal NPs. Electron spin resonance (ESR) measurements at −173 °C were conducted to reveal the charge transport in Ru/TiO_2–H_2 during the light-driven DRM reaction. As shown in Figure 5a, Ru/TiO_2–H_2 displays characteristic oxygen vacancy signals with a g value of 2.003 under vacuum conditions. Notably, illumination can promote the formation of OVs over Ru/TiO_2–H_2 in vacuum, confirmed by the enhanced ESR signal of OVs under light irradiation in Figure 5b. It may be caused by result from light stimulating Ru NPs to generate hot electrons, which then migrate to the conduction band of TiO_2 and react with Ti^{4+} to generate Ti^{3+} and surface oxygen vacancies.[18] The in situ ESR tests were further performed by introducing CO_2 gas into the chamber. When in a CO_2 atmosphere without light irradiation, the signal intensities of OVs remain unchanged in comparison to that in vacuum (Figure 5a), indicating that OVs are not consumed by CO_2 in the dark. However, a significantly decreased signal intensity after introduction of light demonstrates that OVs can activate CO_2 under illumination. The results are consistent with our previous

© 2023 Wiley-VCH GmbH

15213773, 0, Downloaded from https://onlinelibrary.wiley.com/doi/10.1002/anie.202300129 by Cas-Institute Of Urban Environment, Wiley Online Library on [31/03/2023]. See the Terms and Conditions (https://onlinelibrary.wiley.com/terms-and-conditions) on Wiley Online Library for rules of use; OA articles are governed by the applicable Creative Commons License

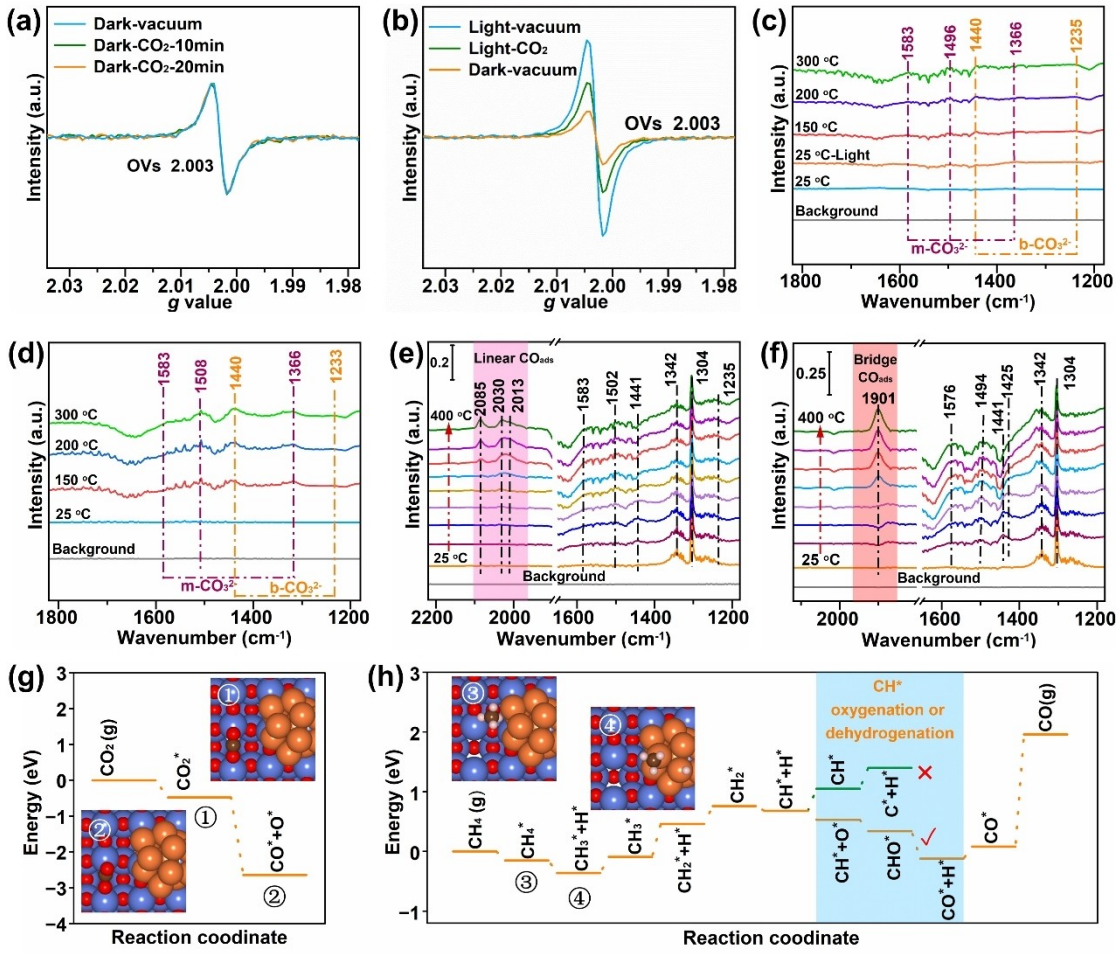

Figure 5. OVs signals of Ru/TiO_2–H_2 during in situ ESR spectroscopy in the a) dark and b) light irradiation, in vacuum and CO_2 atmosphere conditions, respectively. CO_2-DRIFTS spectra of c) Ru/TiO_2–H_2 and d) Ru/TiO_2, respectively. In situ DRIFTS spectra at 400 °C of e) Ru/TiO_2–H_2 and f) Ru/TiO_2, respectively. The gas mixture contains 8 vol% CO_2, 8 vol% CH_4, and 84 vol% Ar. A model of the reaction pathway over Ru/TiO_2 determined from DFT calculations of g) CO_2 dissociation and h) CH_4 decomposition steps. Atom key: C (brown), O (red), H (white), Ru (orange), Ti (blue).

observations and verify that OVs firstly trap the photo-induced electrons, which further facilitate the adsorption and activation of CO_2 molecules.[19] In addition, Ru/TiO_2–H_2 displays a much more intense OV signal compared to Ru/TiO_2 (Figure S14). It means Ru/TiO_2–H_2 possesses more trapping sites to capture electrons from band excitation of TiO_2 or interband transition of Ru, and then endows Ru species with a higher charge-density state under illumination. CO_2 DRIFTS was performed to uncover the CO_2 adsorption and activation route on the catalysts (Figure 5c, d). The band assignments are listed in Table S3. Ru/TiO_2–H_2 displays no intermediate carbonate species at 25 °C. When increasing to 300 °C, the absorption bands ascribed to monodentate carbonate (m-CO_3^{2-}) and bidentate carbonate (b-CO_3^{2-}) occur and the corresponding signal intensities enhance gradually. A similar CO_2 adsorption and activation behavior can also be observed over Ru/TiO_2 catalyst. It reveals that the main active species are m-CO_3^{2-} and b-CO_3^{2-} on the two catalysts, and the increasing temperature is conducive to the formation of carbonate intermediates. Furthermore, the CO_2 DRIFTS of Ru/TiO_2–H_2 under illumination conditions at 25 °C (orange line in Figure 5c) also exhibit the absorption bands of m-CO_3^{2-} and b-CO_3^{2-}, suggesting the light promotion effect on CO_2 activation over Ru/TiO_2–H_2. According to in situ DRIFTS under a DRM atmosphere (Figure 5e, f), both Ru/TiO_2 and Ru/TiO_2–H_2 retain peaks corresponding to CH_3*, m-CO_3^{2-}, and b-CO_3^{2-} species with an increased temperature, which suggests that the adsorption and activation of CO_2 over as-prepared Ru-supported catalysts is not a rate-limiting step, agreeing with the results of CO_2-TPD (Figure S2) and CO_2 DRIFTS. For Ru/TiO_2–H_2, the bands related to adsorbed linear CO are visible at 2085 cm^{-1}, 2030 cm^{-1}, and 2013 cm^{-1}, respectively. Nevertheless, Ru/TiO_2 demonstrates a significantly different CO peak located at 1901 cm^{-1}, which is ascribed to bridged adsorption. Linear CO is generally more readily desorbed at the surface of catalysts than bridging CO, implying that the DRM reaction occurs more easily over Ru/TiO_2–H_2 from the perspective of kinetics. Furthermore, for in situ DRIFTS of Ru/TiO_2–H_2 under illumination (Figure S15), the peak

© 2023 Wiley-VCH GmbH

15213773, 0, Downloaded from https://onlinelibrary.wiley.com/doi/10.1002/anie.202300129 by Cas-Institute Of Urban Environment, Wiley Online Library on [31/03/2023]. See the Terms and Conditions (https://onlinelibrary.wiley.com/terms-and-conditions) on Wiley Online Library for rules of use; OA articles are governed by the applicable Creative Commons License

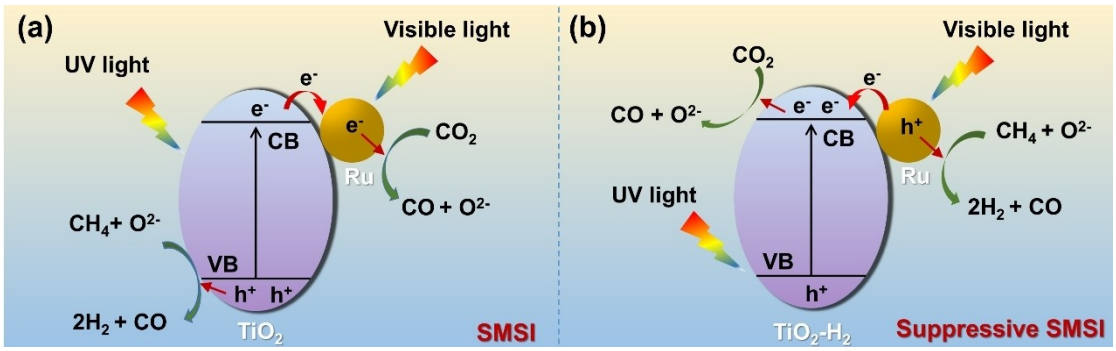

Figure 6. Diagram of light-driven DRM reaction on Ru/TiO_2 and Ru/TiO_2–H_2.

for CO shifts towards a higher wavenumber, which may be a consequence of the light-induced electron-deficient Ru state weakening the interaction between the CO and Ru NPs. This state is conducive to CO desorption and further DRM reaction, which is consistent with the reduced CO activation energy and increased catalytic performance in light-driven DRM catalysis. Next, we examined the catalytic activity over Ru/TiO_2–H_2 under 10 % CH_4/Ar conditions to investigate the mass transport process of oxygen species (Figure S16a, b). Interestingly, both signals of H_2 and CO can be observed and gradually decrease under solely CH_4 conditions. The result is similar to the reported work and indicates that oxygen species in the catalyst can function as the mediator to involve CH_4 dissociation.[20] Density functional theory (DFT) calculations were undertaken to investigate CO_2 (Figure 5g) and CH_4 dissociation (Figure 5h). The modeled Ru/TiO_2 and geometries of CH_4 dissociation steps are shown in Figure S17, and corresponding energies are listed in Tables S4 and S5. The dissociation of C–H bonds in CH_4 is generally deemed as the limiting step in the DRM reaction, while CO_2 is activated to generate O*, which further oxidizes the CH* or C* species to facilitate elimination of the deposited carbon and inhibit catalyst deactivation.[21] The inset geometries images in Figure 5g, h show that the dissociations of CO_2 and CH_4 occur over Ru atoms and the surrounding oxygen vacancies, which thus are deemed as the main active sites for the DRM reaction. Furthermore, the CH* dissociation to C* (CH* dehydrogenation step) located at a high energy barrier is kinetically unfavorable, whereas the energy value of CH* oxidation to CHO* (CH* oxygenation step) is significantly less than that of the CH* dehydrogenation step. Hence, the DRM reaction over Ru/TiO_2 composites occurs mainly via the process of CH* oxidation to CHO*, leading to better resistance to carbon deposition.

According to the above analysis, a reaction mechanism for the photothermal catalytic DRM can be proposed, as displayed in Figure 6a, b. Firstly, light-to-heat conversion provides enough thermal energy to boost the activation of CH_4 and CO_2 in the whole process. Secondly, the light-induced band gap excitation and hot carrier generation compete in Ru/TiO_2 composites, where metal–support interaction strength determines the dominant electron-transfer routes. For Ru/TiO_2 under the light-driven DRM process, the SMSI effect improves the transport efficiency of carriers, and thus excited electrons in the CB of TiO_2 are injected into Ru NPs to yield efficient charge separation. Nevertheless, the charge transfer from TiO_2 to Ru contributes to the high electron density in the Ru surface, which is not conducive to the activation of CH_4 reactant and desorption of CO product, whereas electrophilic CO_2 molecules can be adsorbed and activated by Ru atoms due to the accumulated electrons.[22] Therefore, we speculate that CH_4 tends to react with generated holes in the VB band of TiO_2 for the Ru/TiO_2 catalyst, while CO_2 more likely reacts with the photo-generated electrons on Ru NPs, consistent with the reported reaction model.[23] As for Ru/TiO_2–H_2, due to the weakened SMSI effect, excited electrons in the CB of TiO_2–H_2 and hot electrons with high energies from Ru NPs can be trapped by abundant OVs on the surface of TiO_2–H_2. Consequently, the electron-rich sites can be formed at TiO_2–H_2, whereas the surface electronic state of Ru NPs is positively charged on account of electronic depletion. The electrons gathered in the surface OVs of TiO_2–H_2 mediate the reduction of CO_2* species into CO and O^{2-} by depositing their energy into antibonding orbitals. Meanwhile, for the electron-deficient counterpart, $Ru^{\delta+}$ sites are more likely to accept σ electrons from CH_4 and facilitate C–H bond cleavage to yield H_2 and residual carbon species.[8b] The residual carbon species over Ru NPs can be further eliminated by migrating oxygen ions to generate CO and eventually forming redox looping.[24] Therefore, Ru/TiO_2–H_2 demonstrates superior light-driven photothermal catalytic activities compared to Ru/TiO_2.

Conclusion

The SMSI effect on Ru/TiO_2 induces high charge density in Ru NPs under illumination, which is not favorable for the DRM reaction. By contrast, by pre-annealing commercial P25 in H_2 to adjust the extent of the combination between Ru NPs and TiO_2–H_2, Ru/TiO_2–H_2 shows a significantly enhanced light-driven DRM catalytic performance. The charge transport on Ru/TiO_2–H_2 under illumination is elucidated by KPFM analysis, ISI-XPS analysis, and in situ ESR, and demonstrates that abundant hot electrons excited by the interband transition of Ru transfer to the OVs on

© 2023 Wiley-VCH GmbH

15213773, 0, Downloaded from https://onlinelibrary.wiley.com/doi/10.1002/anie.202300129 by Cas-Institute Of Urban Environment, Wiley Online Library on [31/03/2023]. See the Terms and Conditions (https://onlinelibrary.wiley.com/terms-and-conditions) on Wiley Online Library for rules of use; OA articles are governed by the applicable Creative Commons License

TiO_2–H_2, thus endowing Ru NPs with high chemical state and facilitating CH_4 decomposition. The electrons trapped by OVs serve as the active species to favor CO_2 activation. As a result, both photo-induced thermal effects and photoelectric processes play a crucial role in the light-driven DRM, which overcomes the limitations of the thermal method. The present work paves a way to high-efficiency photothermal catalysts for the DRM reaction through control of the electronic structure.

Acknowledgements

This work was supported by the Strategic Priority Research Program of the Chinese Academy of Sciences [No. XDPB1902], the National Nature Science Foundation of China [No. 21976172], the Science and Technology Planning Project of Fujian Province [2020Y0084], the FJIRSM&IUE Joint Research Fund [No. RHZX-2019-007], and the Youth Innovation Promotion Association of CAS [No. 2021304].

Conflict of Interest

The authors declare no conflict of interest.

Data Availability Statement

The data that support the findings of this study are available from the corresponding author upon reasonable request.

Keywords: CO_2 Reduction · Electronic Transfer Modulations · Photothermal Catalysis · Suppressed Strong Metal-Support Interactions

[1] a) H. Xin, L. Lin, R. Li, D. Li, T. Song, R. Mu, Q. Fu, X. Bao, *J. Am. Chem. Soc.* **2022**, *144*, 4874–4882; b) T. W. van Deelen, C. Hernández Mejía, K. P. de Jong, *Nat. Catal.* **2019**, *2*, 955–970; c) S. C. F. S. J. Tauster, R. L. Garten, *J. Am. Chem. Soc.* **1978**, *100*, 170–175.

[2] a) X. Yang, S. Liu, J. Li, J. Chen, Z. Rui, *Chemosphere* **2020**, *249*, 126096; b) K. Fujiwara, K. Okuyama, S. E. Pratsinis, *Environ. Sci. Nano* **2017**, *4*, 2076–2092.

[3] Z. Luo, G. Zhao, H. Pan, W. Sun, *Adv. Energy Mater.* **2022**, *12*, 2201395.

[4] Y. Guo, Y. Huang, B. Zeng, B. Han, M. Akri, M. Shi, Y. Zhao, Q. Li, Y. Su, L. Li, Q. Jiang, Y. T. Cui, L. Li, R. Li, B. Qiao, T. Zhang, *Nat. Commun.* **2022**, *13*, 2648.

[5] P. Zhou, H. Chen, Y. Chao, Q. Zhang, W. Zhang, F. Lv, L. Gu, Q. Zhao, N. Wang, J. Wang, S. Guo, *Nat. Commun.* **2021**, *12*, 4412.

[6] a) B.-J. Hsieh, M.-C. Tsai, C.-J. Pan, W.-N. Su, J. Rick, H.-L. Chou, J.-F. Lee, B.-J. Hwang, *Electrochim. Acta* **2017**, *224*, 452–459; b) B. M. Stühmeier, R. J. Schuster, L. Hartmann, S. Selve, H. A. El-Sayed, H. A. Gasteiger, *J. Electrochem. Soc.* **2022**, *169*, 034519; c) M. Xu, S. He, H. Chen, G. Cui, L. Zheng, B. Wang, M. Wei, *ACS Catal.* **2017**, *7*, 7600–7609.

[7] a) D. Gao, W. Li, H. Wang, G. Wang, R. Cai, *Trans. Tianjin Univ.* **2022**, *28*, 245–264; b) L. Mascaretti, A. Schirato, T. Montini, A. Alabastri, A. Naldoni, P. Fornasiero, *Joule* **2022**, *6*, 1727–1732; c) D. Pakhare, J. Spivey, *Chem. Soc. Rev.* **2014**, *43*, 7813–7837; d) N. A. K. Aramouni, J. G. Touma, B. A. Tarboush, J. Zeaiter, M. N. Ahmad, *Renewable Sustainable Energy Rev.* **2018**, *82*, 2570–2585.

[8] a) J. Shan, M. Li, L. F. Allard, S. Lee, M. Flytzani-Stephanopoulos, *Nature* **2017**, *551*, 605–608; b) A. I. Olivos-Suarez, À. Szécsényi, E. J. M. Hensen, J. Ruiz-Martinez, E. A. Pidko, J. Gascon, *ACS Catal.* **2016**, *6*, 2965–2981; c) S. M. Kim, P. M. Abdala, T. Margossian, D. Hosseini, L. Foppa, A. Armutlulu, W. van Beek, A. Comas-Vives, C. Coperet, C. Muller, *J. Am. Chem. Soc.* **2017**, *139*, 1937–1949.

[9] H. Song, X. Meng, Z.-j. Wang, Z. Wang, H. Chen, Y. Weng, F. Ichihara, M. Oshikiri, T. Kako, J. Ye, *ACS Catal.* **2018**, *8*, 7556–7565.

[10] J. Liu, C. Li, F. Wang, S. He, H. Chen, Y. Zhao, M. Wei, D. G. Evans, X. Duan, *Catal. Sci. Technol.* **2013**, *3*, 2627–2633.

[11] Y. Zhang, X. Yang, X. Yang, H. Duan, H. Qi, Y. Su, B. Liang, H. Tao, B. Liu, D. Chen, X. Su, Y. Huang, T. Zhang, *Nat. Commun.* **2020**, *11*, 3185.

[12] Y. Guo, S. Mei, K. Yuan, D.-J. Wang, H.-C. Liu, C.-H. Yan, Y.-W. Zhang, *ACS Catal.* **2018**, *8*, 6203–6215.

[13] B. T. Loveless, C. Buda, M. Neurock, E. Iglesia, *J. Am. Chem. Soc.* **2013**, *135*, 6107–6121.

[14] J. Zhou, Z. Gao, G. Xiang, T. Zhai, Z. Liu, W. Zhao, X. Liang, L. Wang, *Nat. Commun.* **2022**, *13*, 327.

[15] a) V. T. Ho, C. J. Pan, J. Rick, W. N. Su, B. J. Hwang, *J. Am. Chem. Soc.* **2011**, *133*, 11716–11724; b) A. V. Tavasoli, M. Preston, G. Ozin, *Energy Environ. Sci.* **2021**, *14*, 3098–3109.

[16] H. Wang, S. Bai, P. Zhao, L. Tan, C. Ning, G. Liu, J. Wang, T. Shen, Y. Zhao, Y.-F. Song, *Catal. Sci. Technol.* **2021**, *11*, 7091–7097.

[17] Z. Rao, Y. Cao, Z. Huang, Z. Yin, W. Wan, M. Ma, Y. Wu, J. Wang, G. Yang, Y. Cui, Z. Gong, Y. Zhou, *ACS Catal.* **2021**, *11*, 4730–4738.

[18] C. Xu, W. Huang, Z. Li, B. Deng, Y. Zhang, M. Ni, K. Cen, *ACS Catal.* **2018**, *8*, 6582–6593.

[19] Q. Li, Y. Gao, J. Chen, H. Jia, *Cell Rep. Phys. Sci.* **2022**, *3*, 101127.

[20] S. Shoji, X. Peng, A. Yamaguchi, R. Watanabe, C. Fukuhara, Y. Cho, T. Yamamoto, S. Matsumura, M.-W. Yu, S. Ishii, T. Fujita, H. Abe, M. Miyauchi, *Nat. Catal.* **2020**, *3*, 148–153.

[21] X. Liu, H. Shi, X. Meng, C. Sun, K. Zhang, L. Gao, Y. Ma, Z. Mu, Y. Ling, B. Cheng, Y. Li, Y. Xuan, Y. Ding, *Sol. RRL* **2021**, *5*, 2100185.

[22] Y. Li, Z. Liu, Z. Rao, F. Yu, W. Bao, Y. Tang, H. Zhao, J. Zhang, Z. Wang, J. Li, Z. Huang, Y. Zhou, Y. Li, B. Dai, *Appl. Catal. B* **2022**, *319*, 121903.

[23] a) M. Kushida, A. Yamaguchi, M. Miyauchi, *J. Energy Chem.* **2022**, *71*, 562–571; b) M. Kushida, A. Yamaguchi, Y. Cho, T. Fujita, H. Abe, M. Miyauchi, *ChemPhotoChem* **2020**, *4*, 275–281; c) Y. Cho, A. Yamaguchi, M. Miyauchi, *Catalysts* **2020**, *11*, 18.

[24] Y. Yang, Z. Chai, X. Qin, Z. Zhang, A. Muhetaer, C. Wang, H. Huang, C. Yang, D. Ma, Q. Li, D. Xu, *Angew. Chem. Int. Ed.* **2022**, *61*, e202200567.

Manuscript received: January 3, 2023
Accepted manuscript online: March 10, 2023
Version of record online: ■■, ■■

© 2023 Wiley-VCH GmbH

15213773, 0, Downloaded from https://onlinelibrary.wiley.com/doi/10.1002/anie.202300129 by Cas-Institute Of Urban Environment, Wiley Online Library on [31/03/2023]. See the Terms and Conditions (https://onlinelibrary.wiley.com/terms-and-conditions) on Wiley Online Library for rules of use; OA articles are governed by the applicable Creative Commons License

Research Articles

CO_2 Reduction Reaction

Q. Li, H. Wang, M. Zhang, G. Li, J. Chen, H. Jia* ——— e202300129

Suppressive Strong Metal-Support Interactions on Ruthenium/TiO_2 Promote Light-Driven Photothermal CO_2 Reduction with Methane

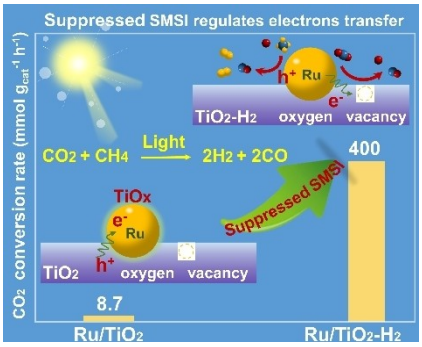

Suppressive strong metal–support interactions (SMSI) enable hot electrons excited on Ru to transfer to a TiO_2–H_2 support, thereby reducing the electron density on Ru to accelerate light-driven CO_2 reduction with methane. The optimized Ru/TiO_2–H_2 composite exhibits an enhanced CO_2 conversion rate of 400 mmol g_{cat}^{-1} h^{-1}.

© 2023 Wiley-VCH GmbH

15213773, 0, Downloaded from https://onlinelibrary.wiley.com/doi/10.1002/anie.202300129 by Cas-Institute Of Urban Environment, Wiley Online Library on [31/03/2023]. See the Terms and Conditions (https://onlinelibrary.wiley.com/terms-and-conditions) on Wiley Online Library for rules of use; OA articles are governed by the applicable Creative Commons License